PILOT COMMAND IMPLEMENTATION IN AIRCRAFTS: A NEW APPROACH BASED ON DYNAMIC INVERSION

Radhakant Padhi*

Abstract

A new approach based on dynamic inversion is proposed in this paper for implementing pilot commands in an aircrafts. The command inputs from the pilot are assumed to be (i) the normal acceleration and forward velocity commands in the longitudinal mode and (ii) roll rate, height and forward velocity commands in the lateral mode. A major difference here is that the second derivatives of the velocities along body y and z directions are assumed to be zero, as opposed to the first derivatives (which is used in many published literature). The new approach leads to a significant reduction of tuning parameters in the control design process, which is a major advantage. Detailed derivations of the modified approach are presented with respect to the generic aircraft dynamics model available in [16]. Extensive Six-DOF simulation studies show that, besides the above advantage, the new approach leads to two other additional advantages; namely reduced oscillatory response and reduced control magnitude. In a comparison study with an existing method using the Six-DOF model for Boeing 747 (with the numerical data available in [16]), numerical results clearly show the improved performance of this new approach. Furthermore, in lateral mode a technique for obtaining a corresponding roll rate command from the desired bank angle command is also implemented. Comparison results show improved performance of the new approach with this modification as well.

Introduction

Designing a control such that the output of an associated system tracks a reference signal is one of the basic and important goals of any controller design. A vast amount of information can be found in the literature addressing various issues related to tracking. If the system is linear and time invariant, relatively easier control design procedures exist for tracking [19]. However, if the system is nonlinear, such control design procedures are still evolving.

Lyapunov based control design techniques [9], [11] use the Lyapunov's stability theorem for nonlinear systems and come up with adaptive control solutions that guarantee asymptotic stability of the error dynamics (i.e. the error goes to zero, implying perfect tracking) or, more often, guarantee "practical stability" (i.e. error remains bounded in a small neighborhood about zero). In sliding mode control [11], [17], the essential idea is to first lay out a path for the error signal that leads to zero. Then the control solution is found in such a way that the error follows this path, finally approaching zero. In doing so, however, the usual problems encountered are high magnitudes of control and control chattering. In Predictive control [18], the error signal is first predicted for some future time (based on a model that may or may not be updated in parallel). The control solution at the current time step is then obtained from an error minimization algorithm that minimizes a cost function, which is a weighted average of the error signal. Use of optimal control theory is also found in the literature for tracking applications. One such approach relies on the error dynamic formulation (with the availability of reference values of all of the states and the associated feed-forward control), thereby essentially reducing it into a regulator problem [5]. An alternate optimal control approach relies on the implicit and explicit model following techniques [2], [7], [19], where the goal is achieved by appropriate formulation of the cost function so that the errors in the output are cancelled out.

A popular method of nonlinear control design for tracking is the technique of dynamic inversion, which is essentially based on the technique of feedback lineariza-

* Assistant Professor, Department of Aerospace Engineering, Indian Institute of Science, Bangalore-560 012, India
Email : padhi@aero.iisc.ernet.in
Manuscript received on 26 Aug 2005; Paper reviewed, revised and accepted on 14 Nov 2005

tion [17]. In this approach, an appropriate co-ordinate transformation is carried out to make the system look linear so that any known linear controller design can be used. A vast amount of literature is available for applications of dynamic inversion control [4], [10], [12]-[15].

A few studies have addressed mismatch between the mathematical model used in the dynamic inversion design and the actual plant. One way of addressing the problem is to augment the dynamic inversion technique with the H_∞ robust control theory [15]. An alternative idea is to adaptively cancel the inversion error with the help of neural network(s), trained [10], [12]. Many benefits of using neural networks for control applications include its ability to effectively control nonlinear plants adapting to unmodeled dynamics and time-varying parameters, simultaneously rejecting the external noise. Interested readers can find many control related applications of neural networks in [8]. With these augmenting tools, the dynamic inversion technique is becoming more powerful and widely popular.

The new method proposed in this paper has features similar to an existing approach [14], where the goal is to design a controller such that the roll rate, normal acceleration and lateral acceleration commands from the pilot are tracked. For turn co-ordination, however, the pilot actually commands the desired roll rate and normal acceleration whereas the lateral acceleration command is kept at zero throughout the maneuvers. However unlike the existing approach, in this paper there is no requirement on transforming the normal and lateral acceleration commands to the pitch and yaw rate commands in the longitudinal mode. In the lateral mode, however, it is assumed that the pilot gives a height command rather than a normal acceleration command. The height command is then transformed into a pitch rate command, which is used for control computation. In order to demonstrate the usefulness of the proposed technique, it is used in a nonlinear Six-Degree-of-Freedom (Six-DOF) model of a transport airplane Boeing-747, for which a limited amount of data is available in [16]. Next, a method to obtain the roll rate command from the desired bank angle command (in lateral mode) is also outlined. Comparative simulation results are presented with respect to this as well, which once again shows that the proposed new method performs better.

Mathematical Formulation for Airplane Control

Six-Degree-of-Freedom Airplane Model

Assuming the airplane to be a rigid body, the complete set of Six-Degree-of-Freedom (Six-DOF) equations of motion over a flat earth in the body frame of reference [16] are:

$$\begin{aligned}
\dot{U} &= VR - WQ - g\sin\Theta + (F_{A_X} + F_{T_X})/m \\
\dot{V} &= WP - UR + g\sin\Phi\cos\Theta + (F_{A_y} + F_{T_y})/m \\
\dot{W} &= UQ - VP + g\cos\Phi\cos\Theta + (F_{A_Z} + F_{T_Z})/m
\end{aligned} \tag{1a}$$

$$\begin{aligned}
\dot{P} &= c_1 QR + c_2 PQ + c_3(L_A + L_T) + c_4(N_A + N_T) \\
\dot{Q} &= c_5 PR - c_6(P^2 - R^2) + c_7(M_A + M_T) \\
\dot{R} &= c_8 PQ - c_2 QR + c_4(L_A + L_T) + c_9(N_A + N_T)
\end{aligned} \tag{1b}$$

$$\begin{aligned}
\dot{\Phi} &= P + Q\sin\Phi\tan\Theta + R\cos\Phi\tan\Theta \\
\dot{\Theta} &= Q\cos\Phi - R\sin\Phi \\
\dot{\Psi} &= (Q\sin\Phi + R\cos\Phi)\sec\Theta
\end{aligned} \tag{1c}$$

$$\begin{bmatrix} \dot{x}_E \\ \dot{y}_E \\ \dot{z}_E \end{bmatrix} = \begin{bmatrix} \cos\Psi & -\sin\Psi & 0 \\ \sin\Psi & \cos\Psi & 0 \\ 0 & 0 & 1 \end{bmatrix} \begin{bmatrix} \cos\Theta & 0 & \sin\Theta \\ 0 & 1 & 0 \\ -\sin\Theta & 0 & \cos\Theta \end{bmatrix} \begin{bmatrix} 1 & 0 & 0 \\ 0 & \cos\Phi & -\sin\Phi \\ 0 & \sin\Phi & \cos\Phi \end{bmatrix} \begin{bmatrix} U \\ V \\ W \end{bmatrix} \tag{1d}$$

where

$$\begin{bmatrix} c_1 \\ c_2 \\ c_3 \\ c_4 \\ c_8 \\ c_9 \end{bmatrix} \triangleq \frac{1}{I_{XX} I_{ZZ} - I_{XZ}^2} \begin{bmatrix} I_{ZZ}(I_{YY} - I_{ZZ}) - I_{XZ}^2 \\ I_{XZ}(I_{ZZ} + I_{XX} - I_{YY}) \\ I_{ZZ} \\ I_{XZ} \\ I_{XZ}^2 + I_{XX}(I_{XX} - I_{YY}) \\ I_{XX} \end{bmatrix} \tag{2a}$$

$$\begin{bmatrix} c_5 & c_6 & c_7 \end{bmatrix} \triangleq (1/I_{YY}) \quad \begin{bmatrix} (I_{ZZ} - I_{XX}) & I_{XZ} & 1 \end{bmatrix} \tag{2b}$$

In Eqs.(1)-(2), U,V,W and $\dot{x}_E, \dot{y}_E, \dot{z}_E$ are the velocity components along the body-fixed and earth-fixed axes respectively, P, Q, R are the roll, pitch and yaw rates respectively about the body-fixed axes, Φ, Θ, Ψ are the

Euler angles. Note that $\dot{h} = -\dot{z}_E$, where h is the height. $F_{A_X}, F_{A_Y}, F_{A_Z}$ are the aerodynamic components and $F_{T_X}, F_{T_Y}, F_{T_Z}$ are the thrust components of the external forces respectively. Similarly, L_A, M_A, N_A are the aerodynamic components and L_T, M_T, N_T are the thrust components of the external moments acting on the airplane. I_{XX}, I_{YY}, I_{ZZ}, I_{XZ} represent the moment of inertias of the airplane in the body frame XYZ. m and g represent mass and acceleration due to gravity respectively (both assumed as constants in this paper). Note that $\dot{\Psi}$, $\dot{x}_E$, $\dot{y}_E$ equations do not couple with other equations due to the flat earth assumption. The thrust components in Eq.(1a,1b) are given by

$$\begin{aligned} F_{T_X} &= \sum_{i=1}^{N} T_i \cos\Phi_{T_i} \cos\Psi_{T_i} \\ F_{T_Y} &= \sum_{i=1}^{N} T_i \cos\Phi_{T_i} \sin\Psi_{T_i} \\ F_{T_Z} &= -\sum_{i=1}^{N} T_i \sin\Phi_{T_i} \end{aligned} \tag{3a}$$

$$\begin{aligned} L_T &= -\sum_{i=1}^{N} \left(T_i \cos\Phi_{T_i} \sin\Psi_{T_i}\right) z_{T_i} - \sum_{i=1}^{N} \left(T_i \sin\Phi_{T_i}\right) y_{T_i} \\ M_T &= \sum_{i=1}^{N} \left(T_i \cos\Phi_{T_i} \cos\Psi_{T_i}\right) z_{T_i} + \sum_{i=1}^{N} \left(T_i \sin\Phi_{T_i}\right) x_{T_i} \\ N_T &= -\sum_{i=1}^{N} \left(T_i \cos\Phi_{T_i} \cos\Psi_{T_i}\right) y_{T_i} \\ &\quad + \sum_{i=1}^{N} \left(T_i \cos\Phi_{T_i} \sin\Psi_{T_i}\right) x_{T_i} \end{aligned} \tag{3b}$$

where T_i is the thrust magnitude of the ith engine, which is located at distances $(x_{T_i}, y_{T_i}, z_{T_i})$ with respect to the origin of the body frame. Φ_{T_i}, Ψ_{T_i} represent the engine orientation angles. Assuming $T_i = \ldots = T_N = T$ and defining a control variable $\sigma_T = T/T_{\max}$, where $T_{\max}$ is the maximum thrust for an engine, we can rewrite Eqs.(3a,3b) as:

$$F_{T_X} = d_1\,\sigma_T, \quad F_{T_Y} = d_2\,\sigma_T, \quad F_{T_Z} = d_3\,\sigma_T \tag{3c}$$

$$L_T = d_4\,\sigma_T, \quad M_T = d_5\,\sigma_T, \quad N_T = d_6\,\sigma_T \tag{3d}$$

where d_1, ..., d_6 are appropriate constants.

The aerodynamic components are computed in the *stability frame* of reference. The rotational transformation matrix from the stability axis to the body axis is

$$T_\alpha \triangleq \begin{bmatrix} \cos\alpha & -\sin\alpha \\ \sin\alpha & \cos\alpha \end{bmatrix} \tag{4}$$

Then, the aerodynamic forces and moments along X, Z directions are given by

$$\begin{bmatrix} F_{A_X} \\ F_{A_Z} \end{bmatrix} = T_\alpha\,(-\bar{q}S) \left(\begin{bmatrix} C_{D_o} & C_{D_\alpha} & C_{D_{ih}} \\ C_{L_o} & C_{L_\alpha} & C_{L_{ih}} \end{bmatrix} \begin{bmatrix} 1 \\ \alpha \\ i_h \end{bmatrix} + \begin{bmatrix} C_{D_{\delta E}} \\ C_{L_{\delta E}} \end{bmatrix} \delta_E \right) \tag{5a}$$

$$\begin{bmatrix} L_A \\ N_A \end{bmatrix} = T_\alpha \begin{bmatrix} L_{A_S} \\ N_{A_S} \end{bmatrix} = T_\alpha \bar{q} S b \left(\begin{bmatrix} C_{l_\beta} \\ C_{n_\beta} \end{bmatrix} \beta + \begin{bmatrix} C_{l_{\delta A}} & C_{l_{\delta R}} \\ C_{n_{\delta A}} & C_{n_{\delta R}} \end{bmatrix} \begin{bmatrix} \delta_A \\ \delta_R \end{bmatrix} \right) \tag{5b}$$

Along the Y direction the aerodynamic component of the force and moment are

$$F_{A_Y} = \bar{q}S\,C_Y = \bar{q}S \left(C_{Y_\beta}\,\beta + \begin{bmatrix} C_{Y_{\delta A}} & C_{Y_{\delta R}} \end{bmatrix} \begin{bmatrix} \delta_A \\ \delta_R \end{bmatrix} \right) \tag{5c}$$

$$M_A = \bar{q}S\bar{c} \begin{bmatrix} C_{m_o} & C_{m_\alpha} & C_{m_{ih}} \end{bmatrix} \begin{bmatrix} 1 & \alpha & i_h \end{bmatrix}^T + C_{m_{\partial E}}\,\delta_E \tag{5d}$$

In Eqs.(4-5), $\alpha = \tan^{-1}(W/U)$ represents the angle of attack, $\beta = \sin^{-1}(V/V_T)$ (where $V_T = \sqrt{U^2 + V^2 + W^2}$ is the airspeed) represents the side-slip angle and $\bar{q} = (1/2)\,\rho V_T^2$ represents the dynamic pressure. δ_A, δ_E, δ_R are the aileron, elevator and rudder deflections respectively. S, $\bar{c}$, b are the wetted area, mean aerodynamic chord and wing span respectively.

$$C_{D_o}, C_{D_\alpha}, C_{D_{i_h}}, C_{L_o}, C_{L_{i_h}},$$

$$C_{D_{\delta_E}}, C_{L_{\delta_E}}, C_{l_\beta}, C_{n_\beta}, C_{l_{\delta_A}}, C_{l_{\delta_R}}, C_{n_{\delta_A}}, C_{n_{\delta_R}},$$

$$C_{Y_\beta}, C_{Y_{\delta_A}}, C_{Y_{\delta_R}}, C_{m_o}, C_{m_\alpha}, C_{m_{i_h}},$$

and $C_{m_{\delta_E}}$, are the aerodynamic derivatives. Typically they vary with the flight conditions and are available in a tabular form as a function of some flight scheduling variables (typically height, dynamic pressure and Mach number etc.). In this research the values of these are taken from [16] for low altitude (20,000 ft) cruise condition and they are assumed to remain constant during the maneuvering time. The engine data, however, was taken from the Boing website. One may find more details about the meanings of these aerodynamic derivatives in [16]. Using Eqs.(3-5), Eqs.(1a,b) can be rewritten as

$$\dot{X}_V = f_v(X) + \left[g_v(X)\right] U_c = \left[f_{v_1}(X) + f_{v_2}(X_p)\right] + \left[g_v(X)\right] U_c \tag{6a}$$

$$\dot{X}_R = f_R(X) + \left[g_R(X)\right] U_c = \left[f_{R_1}(X) + f_{R_2}(X_p)\right] + \left[g_R(X)\right] U_c \tag{6b}$$

where

$$X \triangleq [U\ V\ W\ P\ Q\ R\ \Phi\ \Theta\ h\ ]^T,$$

$$X_V \triangleq [U\ V\ W]^T,$$

$$X_R \triangleq [P\ Q\ R]^T,$$

$$X_P \triangleq [\alpha\ \beta\ \bar{q}\ M]^T,$$

$$U_c \triangleq \left[\delta_A\ \delta_E\ \delta_R\ \sigma_T\right]^T,$$

Note that M represents the Mach number. Other terms are defined as follows :

$$f_{v_1}(X) = \begin{bmatrix} VR - WQ - g\sin\Theta \\ WP - UR + g\sin\Phi\cos\Phi \\ UQ - VP + g\cos\Theta\cos\Phi \end{bmatrix} \tag{7a}$$

$$f_{R_1}(X) = \begin{bmatrix} c_1 QR + c_2 PQ \\ c_5 PR - c_6(P^2 - R^2) \\ c_8 PQ - c_2 QR \end{bmatrix} \tag{7b}$$

$$f_{v_2}(X_p) = \left[a_{11}\ a_2\ a_{12}\right]^T \tag{7c}$$

$$g_V(X) = \begin{bmatrix} 0 & b_{11} & 0 & d_1/m \\ b_{21} & 0 & b_{22} & d_2/m \\ 0 & b_{12} & 0 & d_3/m \end{bmatrix} \tag{7d}$$

$$f_{R_2}(X_p) = \left[a_{31}\ a_4\ a_{32}\right]^T \tag{7e}$$

$$g_R(X) = \begin{bmatrix} b_{31} & 0 & b_{32} & (c_3 d_4 + c_4 d_6) \\ 0 & b_4 & 0 & c_7 d_5 \\ b_{33} & 0 & b_{34} & (c_4 d_4 + c_9 d_6) \end{bmatrix} \tag{7f}$$

where

$$\begin{bmatrix} a_{11} \\ a_{12} \end{bmatrix} \triangleq -(\bar{q}S/m) T_\alpha \begin{bmatrix} C_{D_o} & C_{D_\alpha} & C_{D_{ih}} \\ C_{L_o} & C_{L_\alpha} & C_{L_{ih}} \end{bmatrix} \begin{bmatrix} 1 \\ \alpha \\ i_h \end{bmatrix} \tag{8a}$$

$$\alpha_2 \triangleq (\bar{q}S/m)\, C_{y_\beta} \beta \tag{8b}$$

$$\left[b_{11}\ b_{12}\right]^T \triangleq -(\bar{q}S/m) T_\alpha \left[C_{D_{\delta E}}\ C_{L_{\delta E}}\right]^T \tag{8c}$$

$$\left[b_{21}\ b_{22}\right]^T \triangleq (\bar{q}S/m) \left[C_{y_{\delta A}}\ C_{y_{\delta R}}\right] \tag{8d}$$

$$\begin{bmatrix} a_{31} \\ a_{32} \end{bmatrix} \triangleq \begin{bmatrix} c_3 & c_4 \\ c_4 & c_9 \end{bmatrix} T_\alpha \bar{q} S b \begin{bmatrix} C_{l_\beta} \\ C_{n_\beta} \end{bmatrix} \beta \tag{8e}$$

$$\begin{bmatrix} b_{31} & b_{32} \\ b_{33} & b_{34} \end{bmatrix} \triangleq \begin{bmatrix} c_3 & c_4 \\ c_4 & c_9 \end{bmatrix} T_\alpha \bar{q} S b \begin{bmatrix} C_{l_{\delta A}} & C_{l_{\delta R}} \\ C_{n_{\delta A}} & C_{n_{\delta R}} \end{bmatrix} \tag{8f}$$

$$a_4 \triangleq c_7 \bar{q} S \bar{c} \left[C_{m_o}\ C_{m_{ih}}\ C_{m_\alpha}\right] [1\ \ i_h\ \ \alpha]^T \tag{8g}$$

$$b_4 \triangleq c_7 (\bar{q} S \bar{c})\, C_{m_{\delta E}} \tag{8h}$$

The normal acceleration (n_z) and the lateral acceleration (n_y) are defined as [14]

$$n_z \triangleq -(F_z/m) \tag{9a}$$

$$n_y \triangleq (F_y/m) \tag{9b}$$

In Eq.(9), $F_z = F_{A_z} + F_{T_z}$, $F_y = F_{A_y} + F_{T_y}$ are the aerodynamic and thrust forces acting on the airplane along the body *z* and *y* directions respectively. With the definitions

in Eq.(9), the system dynamics along the body z and y directions can be written as

$$n_z = UQ - VP + g\cos\Phi\cos\Theta - \dot{W} \tag{10a}$$

$$n_y = UR - WP - g\sin\Phi\cos\Theta + \dot{V} \tag{10b}$$

Alternatively, these quantities can also be written as

$$n_z = f_{n_z} + g_{n_z} U_c \tag{11a}$$

$$n_y = f_{n_y} + g_{n_y} U_c \tag{11b}$$

where

$$\begin{bmatrix} f_{n_z} & f_{n_y} \end{bmatrix}^T \triangleq [-a_{12} \quad a_2]^T \tag{12a}$$

$$\begin{bmatrix} g_{n_z} \\ g_{n_y} \end{bmatrix} \triangleq \begin{bmatrix} 0 & -b_{12} & 0 & -d_3/m \\ b_{21} & 0 & b_{22} & d_2/m \end{bmatrix} \tag{12b}$$

Also note that from Eq.(6a, 6b) one can write :

$$\dot{U} = f_U(X) + g_U(X)\, U_c \tag{13}$$

$$\dot{P} = f_P(X) + g_P(X)\, U_c \tag{14}$$

$$\dot{Q} = f_Q(X) + g_Q(X)\, U_c \tag{15}$$

where

$f_U(X) \triangleq f_V(1,:),\ g_U(X) \triangleq g_V(1,:), f_P(X) \triangleq f_R(1,:),$
$g_P(X) \triangleq g_R(1,:),\ f_Q(X) \triangleq f_R(2,:),\ g_Q(X) \triangleq g_R(2,:).$

Synthesis of Controller Using Dynamic Inversion

In [10], [12], [14], the objective is to design a controller such that the roll rate $P \to P^*$, normal acceleration $n_z \to n_z^*$ and lateral acceleration $n_y \to n_y^*$ where P^*, n_z^*, n_y^* are the commanded values from the pilot. For turn co-ordination, however, the pilot actually commands P^* and n_z^*, whereas the lateral acceleration command $n_y^* = 0$ throughout the maneuver. Note that in pure longitudinal maneuvers $P^* = 0$.

It should be noted that the $\dot{W}$and $\dot{V}$ terms in Eqs.(10a,10b) complicates the procedure of command transformation to body rates of rotation. In [14], n_z, n_y are replaced by proportional and integral error terms in the Command Augmentation System (an outer loop) and, more importantly, it is assumed that $\dot{W} = \dot{V} = 0$. Eqs.(10a-10b) are then used to solve for $Q = Q^*$and $R = R^*$, which along with the commanded value of $P = P^*$serve as the command inputs $\begin{bmatrix} P^* & Q^* & R^* \end{bmatrix}^T$ to the Attitude Control Logic (an inner loop) that is used in solving for control . It is also assumed that $\begin{bmatrix} \ddot{\Phi}^* & \ddot{\Theta}^* & \ddot{\Psi}^* \end{bmatrix}^T = 0$. For completeness of this paper, this technique is briefly outlined in the appendix.

In order to cancel the errors caused due to the approximation that $\dot{W} = \dot{V} = 0$, an integral feedback is used. Since it may lead to "*control wind-up*", an associated wind-up prevention logic is needed. In this paper, the need for an intermediate command transformation and the need to introduce any integral feedback for the errors in acceleration commands are eliminated. it is assumed that $\ddot{W} = \ddot{V} = 0$, a more realistic assumption compared to assuming $\dot{W} = \dot{V} = 0$. Moreover, the additional assumption $\begin{bmatrix} \ddot{\Phi}^* & \ddot{\Theta}^* & \ddot{\Psi}^* \end{bmatrix}^T = 0$ is also not necessary.

First, we define new variables a_z, a_z^* and a_y, a_y^*as

$$a_z \triangleq n_z + \dot{W}, \quad a_z^* \triangleq n_z^* + \dot{W} \tag{16a}$$

$$a_y \triangleq n_y - \dot{V}, \quad a_y^* \triangleq n_y^* - \dot{V} \tag{16b}$$

The new method relies on the key observation that $\left(\begin{bmatrix} n_z & n_y \end{bmatrix}^T \to \begin{bmatrix} n_z^* & n_y^* \end{bmatrix}^T \right) \Leftrightarrow \left(\begin{bmatrix} a_z & a_y \end{bmatrix}^T \to \begin{bmatrix} a_z^* & a_y^* \end{bmatrix}^T \right)$; this is because of the one-to-one correspondence between them. From Eqs.(10a,10b) and (16a,10b), it can be seen that

$$a_z = UQ - VP + g\cos\Phi\cos\Theta \tag{17a}$$

$$a_y = UR - WP - g\sin\Phi\cos\Theta \tag{17b}$$

Taking derivatives of both sides with respect to time and using Eqs.(1c) and (6a,6b), we get

$$\dot{a}_z = f_{a_z}(X) + g_{a_z}(X)\, U_c \tag{18a}$$

$$\dot{a}_y = f_{a_y}(X) + g_{a_y}(X)\, U_c \tag{18b}$$

where

$$\begin{bmatrix} f_{a_z} & f_{a_y} \end{bmatrix}^T \triangleq \begin{bmatrix} A_1 + B_1 f_V + C_1 f_R \end{bmatrix} \tag{19a}$$

$$\begin{bmatrix} g_{a_z}^T & g_{a_y}^T \end{bmatrix}^T \triangleq B_1 g_V + C_1 g_R \tag{19b}$$

$$A_1 \triangleq g \begin{bmatrix} -\sin\Phi\cos\Theta & -\cos\Phi\sin\Theta \\ -\cos\Phi\cos\Theta & \sin\Phi\sin\Theta \end{bmatrix} \begin{bmatrix} \dot{\Phi} \\ \dot{\Theta} \end{bmatrix} \tag{19c}$$

$$B_1 \triangleq \begin{bmatrix} Q & -P & 0 \\ R & 0 & -P \end{bmatrix} \tag{19d}$$

$$C_1 \triangleq \begin{bmatrix} -V & U & 0 \\ -W & 0 & U \end{bmatrix} \tag{19e}$$

Longitudinal Maneuvers

In this case the goal is $X_T \to X_T^*$, where $X_T \triangleq \begin{bmatrix} P & n_z & n_y & U \end{bmatrix}$, $X_T^* \triangleq \begin{bmatrix} P^* = 0 & n_z^* & n_y^* = 0 & U^* \end{bmatrix}$. Defining $\hat{X}_T \triangleq \left(X_T - X_T^* \right)$, a controller is designed such that the stable error dynamics has the following structure.

$$\dot{\hat{X}}_T + K \hat{X}_T = 0 \tag{20}$$

where the gain matrix K is selected to be a positive definite matrix. A relatively easier way to select the gain matrix K is to choose the i^{th} diagonal element to be $1/\tau_i$, where $\tau_i > 0$ is the desired *time constant* of the i^{th} channel of the error dynamics. In this study, the gain K is selected as

$$K = diag\,(1/\tau_P, 1/\tau_{n_z}, 1/\tau_{n_y}, 1/\tau_U) \tag{21}$$

With the assumption $\ddot{W} = \ddot{V} = 0$, from Eq.(16a), it is clear that $\begin{bmatrix} \dot{n}_z & \dot{n}_y \end{bmatrix} = \begin{bmatrix} \dot{a}_z & \dot{a}_y \end{bmatrix}$ and from Eqs.(13-14) and (18a,18b),

$$\begin{bmatrix} f_P + g_P U_c \\ f_{a_z} + g_{a_z} U_c \\ f_{a_y} + g_{a_y} U_c \\ f_U + g_U U_c \end{bmatrix} - \dot{X}_T^* + K \left\{ X_T + \begin{bmatrix} 0_{1\times 3} \\ g_{n_z} \\ g_{n_y} \\ 0_{1\times 3} \end{bmatrix} U_c - X_T^* \right\} = 0 \tag{22}$$

Rearranging terms and carrying out the necessary algebra, an expression for the controller reduces to

$$U_c = A_U^{-1}\, b_U \tag{23}$$

where

$$A_U \triangleq \begin{bmatrix} g_P^T & g_{a_z}^T & g_{a_y}^T & g_U^T \end{bmatrix}^T + K \begin{bmatrix} 0^T & g_{n_z}^T & g_{n_y}^T & 0^T \end{bmatrix}^T \tag{24a}$$

$$b_U \triangleq -\begin{bmatrix} f_P & f_{a_z} & f_{a_y} & f_U \end{bmatrix}^T - K \begin{bmatrix} X_T - X_T^* \end{bmatrix} + \dot{X}_T^* \tag{24b}$$

It is assumed here that the matrix A_U is invertible for $\forall$t during the application of control. Note that this assumption may or may not remain valid $\forall$t in practical implementation, since the matrix elements keep on changing during the flight. However, a typical way to overcome this problem is to implement the control update only if $abs\,(\,|A_U|) > tol$, where *tol* is a user defined tolerance value. Obviously this may degrade the performance of the controller, but it will avoid the major problems in connection with the singular A_U matrix. Even though such a precaution was implemented in the numerical experiment, A_U was never found to violate this condition in the numerous simulation studies.

An implementation schematic of the controller in Eqs.(23)-(24) is given in Fig.1.

Lateral Maneuvers

During lateral maneuvers, an appropriate time-varying n_z^* is needed to maintain constant altitude. Consequently, the objectives in this mode are to drive $P \to P^*$, $n_y \to n_y^* = 0$, $U \to U^*$ and height $h \to h^*$, where h^* is the commanded height. That is to assure that $X_T \to X_T^*$, where $X_T \triangleq \begin{bmatrix} P & h & n_y & U \end{bmatrix}^T$ and $X_T^* \triangleq \begin{bmatrix} P^* & h^* & n_y^* = 0 & U^* \end{bmatrix}^T$.

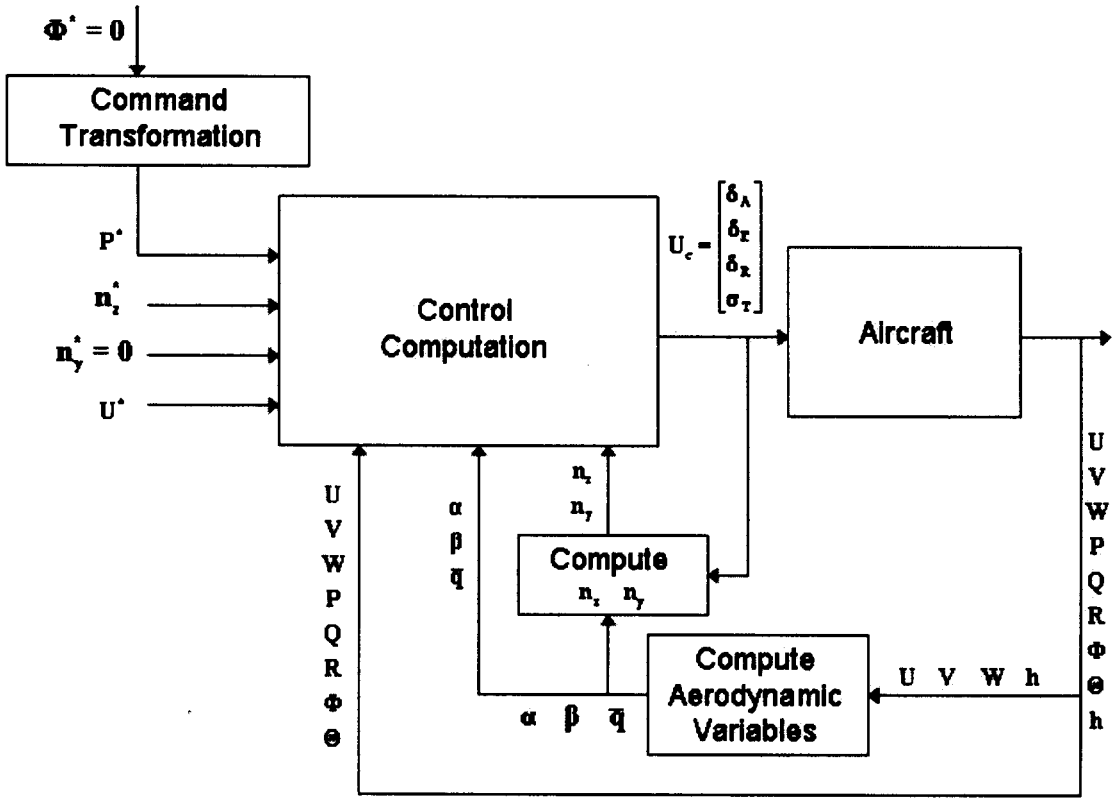

Fig.1 Implementation of the new logic in longitudinal mode

Note that the appropriate n_z^* is automatically computed in this process. However, from Eq.(1d) we observe that the control U_c does not appear in the $\dot{h}$ equation. As a result, an error expression is defined first as $\hat{h} \triangleq (h - h^*)$ and a stable height-error dynamics is formulated as

$$\dot{\hat{h}} + (1/\tau_h)\,\hat{h} = 0 \tag{25}$$

where $\tau_h > 0$ is the desired time constant. By substituting for $\dot{h}$ from Eq.(1d), this can be expanded as

$$[U \sin\Theta - V\cos\Theta \sin\Phi - W\cos\Theta\cos\Phi] - \dot{h}^* + (1/\tau_h)\,(h - h^*) = 0 \tag{26}$$

Solve for Θ (and denote it as Θ^*) from Eq.(26) with a nonlinear equation solver (e.g. Newton-Raphson technique [6]).

Similarly, a stable first-order error dynamics is constructed for the pitch angle by defining $\hat{\Theta} = (\Theta - \Theta^*)$.

$$\dot{\hat{\Theta}} + (1/\tau_\Theta)\,\hat{\Theta} = 0 \tag{27}$$

where $\tau_\Theta > 0$ is the desired time constant. Substituting for $\dot{\Theta}$ equation from Eq.(1c) and assuming Θ^* to be constant at each instant of time (quasi-steady assumption), an expression for Q (and denote it as Q^*) can be obtained as

$$Q^* = (1/\cos\Phi)\left[R\sin\Phi - (1/\tau_\Theta)\,(\Theta - \Theta^*)\right] \tag{28}$$

The pitch rate Q^* is assumed to be quasi-steady (held constant at each instant of time). Since U_c appears in the $\dot{Q}$ equation (15), it facilitates control computation as follows: First, re-define $X_T \triangleq \left[P \;\; Q \;\; n_y \;\; U\right]^T$, $X_T^* \triangleq \left[P^* = 0 \;\; Q^* \;\; n_y^* = 0 \;\; U^*\right]^T$

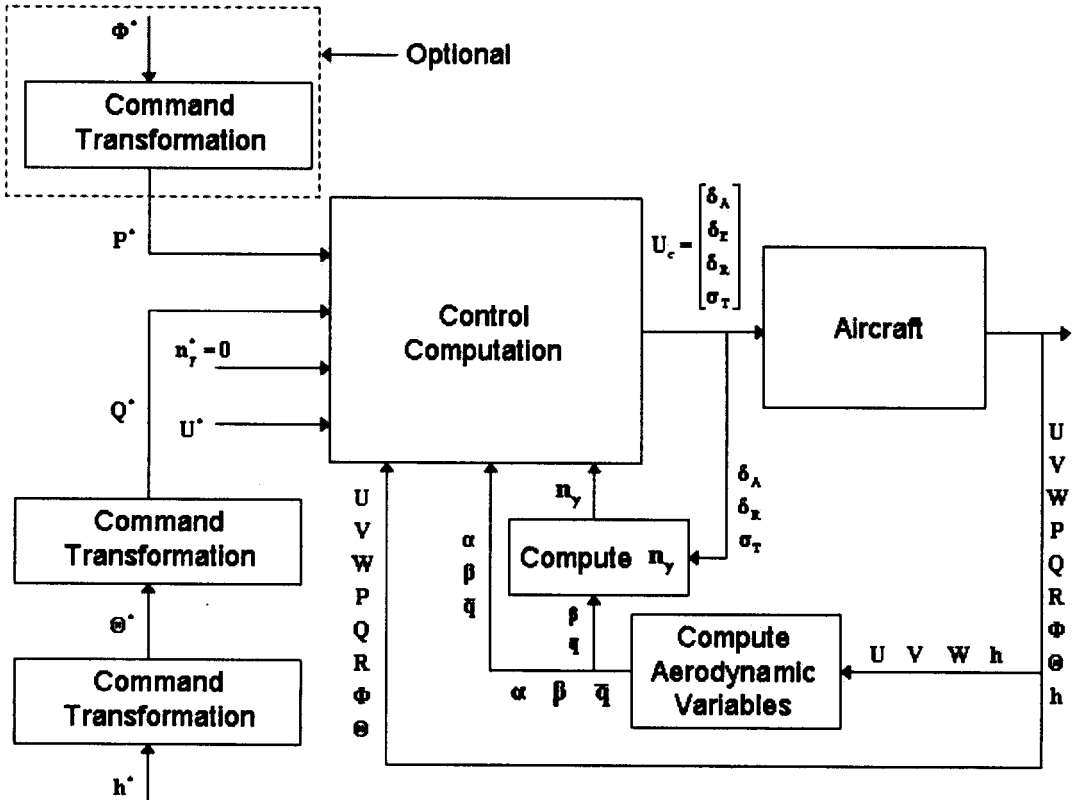

Fig.2 Implementation of the new logic in lateral mode

and $\hat{X}_T \triangleq \left(X_T - X_T^*\right)$ The objective now is to synthesize a controller such that Eq.(20) is satisfied. In this case, the gain matrix is selected to be of the form

$$K = diag\,(1/\tau_P,\ 1/\tau_Q,\ 1/\tau_{n_y},\ 1/\tau_U) \tag{29}$$

Following the steps outlined before and carrying out the necessary algebra, an expression for control can be written in the following form

$$U_c = A_U^{-1}\, b_U \tag{30}$$

where

$$A_U \triangleq \left[g_P^T \;\; g_Q^T \;\; \left(g_{a_y}^T + (1/\tau_{n_y})\; g_{n_y}^T\right) \;\; g_U^T\right]^T \tag{31a}$$

$$b_U \triangleq -\left[f_P \;\; f_Q \;\; f_{a_y} \;\; f_U\right]^T - K\left[X_T - X_T^*\right] \tag{31b}$$

Note that the command transformation from h^* to Q^* can be considered as an outer-loop, whereas the subsequent control computation can be interpreted as an inner-loop. However, due to the quasi-steady assumptions, one should guarantee $\tau_h > \tau_\Theta > \tau_Q$, so that *the inner-loop dynamics is faster than the outer-loop dynamics*. Implementation of this idea is presented in a flow chart in Fig.2.

Numerical Experiments

Selection of Numerical Values

All numerical data used (in SI units) are for a Boeing-747 transport airplane at a low-cruise altitude (20,000 *ft* = 6.096 *km*) [16]. Note that only a limited amount of vehicle and aerodynamic data is available in [16] and that is what has been used in the simulation studies. Moreover, since the engine data is not available in [16], maximum values for engine thrusts and values for engine orientations were obtained from the Boeing website and an appropriate value of the actual thrust was adjusted from a trim routine (see below). A fourth-order Runge-Kutta technique [6] with fixed step size (0.05 Sec) was used for numerical integration.

Trim Condition

In order to obtain a *trim condition*, it was assumed that the airplane was initially flying at a straight level flight at the known cruise altitude (h = 20,000 *ft* = 6096 m). That is $P = Q = R = 0$ and $\Phi = 0$. The engines are assumed to operate at a known percentage of their maximum value. Then, by using Eq.(1a,1b,1d), the variables $\left[U\ V\ W\ \Theta\ \delta_A\ \delta_E\ \delta_R\right]^T$ were solved for from the $\left[\dot{U}\ \dot{V}\ \dot{W}\ \dot{P}\ \dot{Q}\ \dot{R}\ \dot{h}\right]^T = 0$ equation, with a Newton-Raphson nonlinear equation solver [6]. The trim condition values, when all of the four engines operate at 23.5% of their maximum value (which is 43,000 *lb* = 1.935 x 10^5 *N*), are *U* = 205.6538 *m*/sec, *V* = 0 *m*/sec, *W* = 9.563 *m*/sec, *P* = *Q* = *R* = 0 deg/sec, Φ = 0 deg, Θ = 2.6623 deg. The domain for our initial conditions for this study were defined to be close to the trim values (since exact trim conditions are practically unrealistic). Note that once the atmospheric pressure and density variations with height is known, $[U\ V\ W\ h]^T$ and $[\alpha\ \beta\ \bar{q}\ h]^T$ can be interchanged. Furthermore, knowing *h* and *M*, $\bar{q}$ can be computed. The trim conditions for α, β, *h* and *M* are given by 2.6624 deg, 0 deg, 6096 m and 0.6615 respectively. Next, since the exact trim condition may not be realized in practice, the domain for initial condition is chosen as

$P \in$ [-0.1, 0.1] deg/sec, $Q \in$ [-0.1, 0.1] deg/sec,
$R \in$ [-0.1, 0.1] deg/sec $\alpha \in$ [+2.5, 2.8] deg,
$\beta \in$ [-0.1, 0.1] deg, $M \in$ [0.64 0.66],
$h \in$ [-19,500 20,500] *ft* = [5943.6 6248.4]*m*
$\Phi \in$ [-0.1, 0.1] deg, $\Theta \in$ [2.5, 2.8] deg.

Random values were chosen from the above domains to obtain initial conditions for simulation purpose.

Selection of Control Design Parameters

After some trial and error the following values were selected for the time constants: $\tau_P = 1$, $\tau_{n_z} = 1$, $\tau_{n_y} = 1$, and $\tau_U = 50$ in the longitudinal case and $\tau_P = 1$, $\tau_h = 50$, $\tau_\Theta = 10$, $\tau_Q = 1$, $\tau_{n_y} = 1$and $\tau_U = 50$ in the lateral case. The choice of these values was mainly guided by the compromise between the speed of response and the associated control histories.

In order to compare the performance of the modified formulation with the existing version [14] (see appendix for a summary of it), gain values of $k_1 = k_3 = 1$, $k_2 = k_4 = 2$ were selected for the command augmentation system. Similarly in the attitude orientation system, parameter values of $k_{v_i} = 2\,\zeta_i\,\omega_{n_i}$, $k_{P_i} = \omega_{n_i}^2$, with $\zeta_i = 0.5$, $\omega_{n_i} = 2$ rad/sec (i = 1,2,3) were selected for each of the attitude angle error dynamic channels and the time constants $\tau_U = 50$ for this case as well.

It is important to point out that the existing technique need *eleven* design parameters in longitudinal case and *twelve* in the lateral case. In the new approach presented in this study only *four* are needed for the longitudinal mode and only *six* are needed for the lateral case. This significantly less number of design parameters without compromising in performance is clearly a potential advantage of the new approach.

Analysis of Results

In our numerical studies, the goal was to track the reference commands for 60 Sec. At 20 Sec. interval, the command was altered to reflect possible real life scenarios. In all plots, the solid lines represent the results from the new approach presented in this paper, where as the dashed lines represent the results from the existing approach [14].

Longitudinal Maneuver

In Figs.3-8, simulation results for a lateral maneuver are presented. The initial conditions are picked arbitrarily from the domain considered. The commanded values of the normal accelerations are typically small for transport airplanes. The maximum value of n_z^* for such airplanes

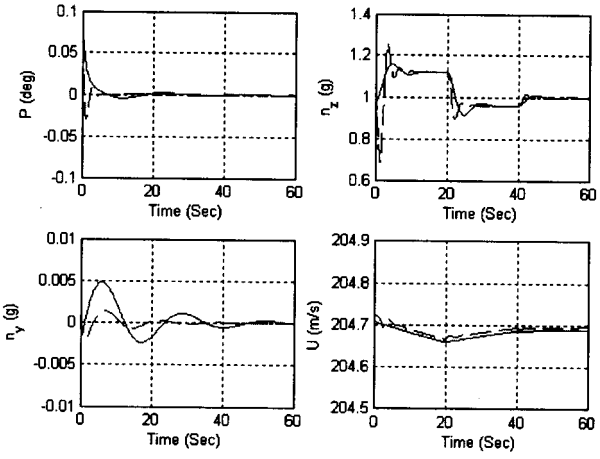

Fig.3 Roll rate, Normal acceleration and Lateral acceleration in longitudinal maneuver

recommended [10] is 1.12g. The following sequence of command signals is input: $\left[P^* \;\; n_z^*\right]$ = [0 1.12g] for t ∈ [0, 20] Sec, $\left[P^* \;\; n_z^*\right]$ = [0 0.88g] for t ∈ [20, 40] Sec and $\left[P^* \;\; n_z^*\right]$ = [0 1.0g] for t ∈ [40, 60] Sec. Throughout the maneuver, it is assumed that $U^* = U_0$ (the initial condition value) and $n_y^* = 0$.

In Fig.3, observe that the roll rate goes to zero quickly and lateral acceleration remains very close to zero throughout the maneuver. It is clear that the goal of normal acceleration tracking is met for both approaches. However, the new approach offers several improvements. First, the transient oscillations have much smaller overshoot and the frequency of oscillation is less (which is also evident from the pitch rate history in Fig.5). This leads to better handling quality of the airplane. From Fig.1, it can also be observed that even though the normal acceleration is eventually tracked in the existing approach successfully, initially it shows a non-minimum phase behavior (i.e. the initial response is in the opposite direction with respect to the command).

From Fig. 4 it is evident that the control surface deflections are not high in both the approaches. However, the initial elevator deflection requirement is of much smaller magnitude in the new approach. Moreover, the existing approach exhibits some high-frequency oscillations in the elevator and thrust controls whereas with the new approach these control trajectories are comparatively much smoother. The sharp changes in the control plots can be attributed to absence of actuator dynamics in the model.

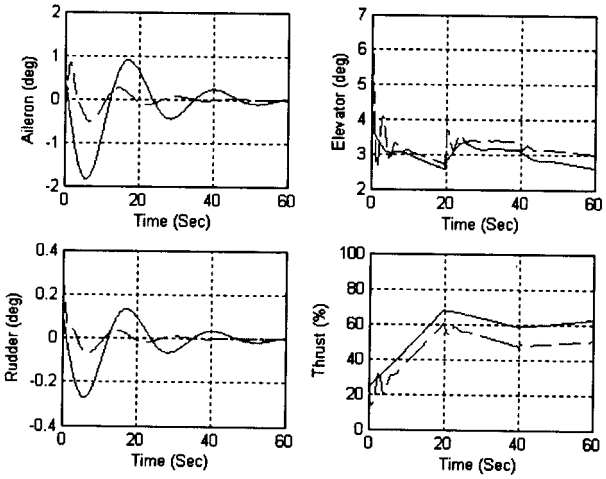

Fig.4 Aileron, Elevator and Rudder deflections and Thrust in longitudinal maneuver

For completion, trajectories of roll, pitch and yaw rates are presented in Fig.5, aerodynamic variables are presented in Fig.6, velocity components and height histories are presented in Fig.7 and Euler angles are presented in Fig.8. From these figures it is clear that all the non-tracked state variables remain within reasonable values throughout the maneuver. Simulation studies for a large number of cases did not show instability in any of the cases.

Lateral Maneuver

Simulation results for a lateral maneuver from an arbitrary initial condition are presented in Figs. 9-15. The sequence of command signals applied consisted of

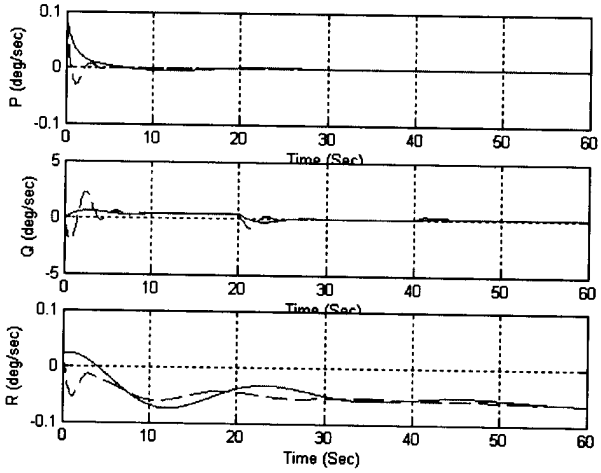

Fig.5 Roll, Pitch and Yaw rates in longitudinal maneuver

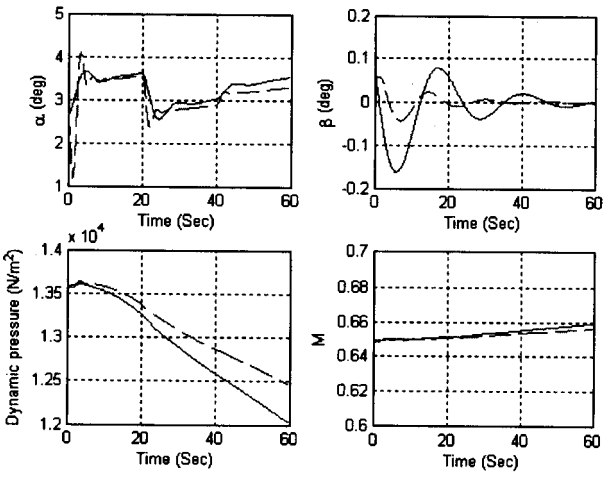

Fig.6 Aerodynamic variables in longitudinal maneuver

P^* = 2.8 deg/sec $t \in$ [0, 20] sec, P^* = -2.8 deg/sec $t \in$ (20, 40) sec and P^* = 0 deg/sec for $t \in$ [40, 60] sec. Throughout the maneuver it was assumed that $U^* = U_0$, $h^* = h_0$ (the initial condition values) and $n_y^* = 0$. However, the pilot can essentially select any other reasonable values.

Note that the lateral accelerations in both approaches remain close to zero (which is also evident in small side-slip angle in Fig.13), which was a requirement for the maneuvers. However, in the new approach both lateral acceleration and side-slip angles remain more close to zero. In other words, it leads to better turn-coordination. For clarity, the aileron and rudder control plots of Fig.10 in Fig.11 are zoomed in a region. Observe that in the existing approach at 20 sec, the aileron deflection is quite high. Furthermore, a low thrust of about 10% of the maximum value might also be of some concern from safety considerations (as the engine may possibly shut down). Besides, in the existing approach the elevator and rudder deflection histories show high frequency transient oscillations; this should preferably be avoided. These trends are absent in the performance of the modified approach. The control surface histories are relatively smaller and smoother. Moreover, the thrust control value remains above 20% of the maximum value throughout the maneuver, which is an additional advantage. We have plotted all other state and aerodynamic variables in Figs.12-15. Once again it is clear that all of these variables remain within reasonable limits for the duration of the maneuvers.

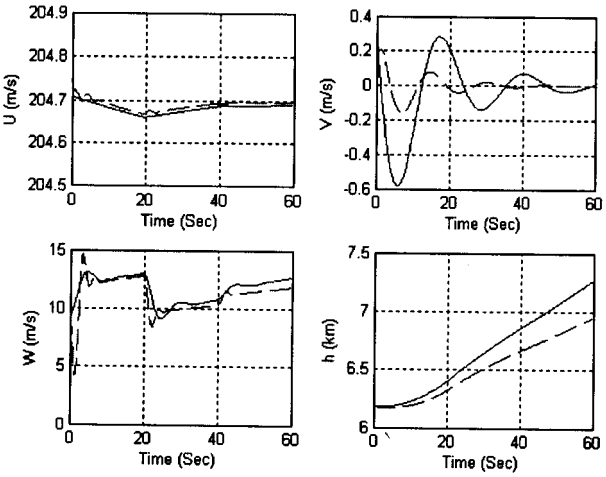

Fig.7 Velocity components and height in longitudinal maneuver

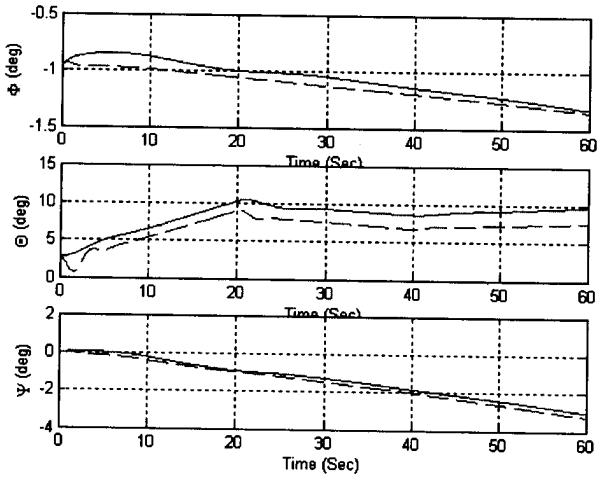

Fig.8 Euler angles in longitudinal maneuver

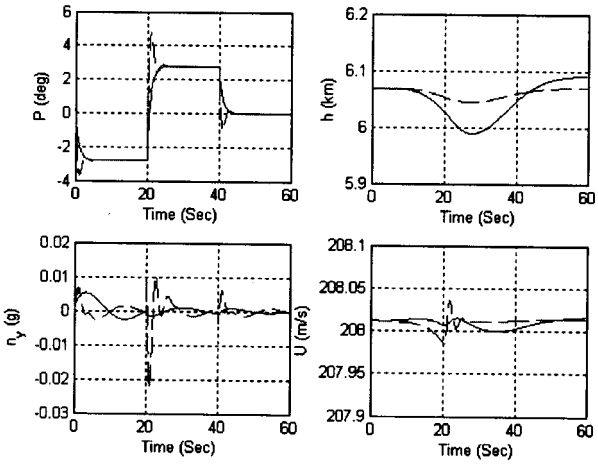

Fig.9 Roll rate, Normal acceleration and Lateral acceleration in lateral maneuver

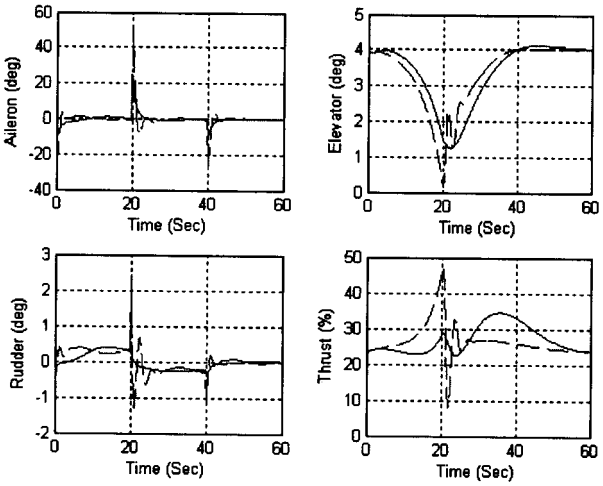

Fig.10 Aileron, Elevator and Rudder deflections and Thrust level in lateral maneuver

Implementation of Bank Angle Command

Even though P^* can be assumed as a constant [12], [14], a constant roll-rate command cannot be applied for a long duration of time, which is especially true for transport aircrafts as the aircraft is not supposed to roll continuously. an alternative idea of generating the roll rate command P^* from a bank-angle command Φ^* is described in this section. First define the error $\hat{\Phi} \triangleq \left(\Phi - \Phi^*\right)$ and let the desired error dynamics be

$$\dot{\hat{\Phi}} + (1/\tau_\Phi)\,\hat{\Phi} = 0, \quad \tau_\Phi > 0 \tag{32}$$

By substituting for $\dot{\Phi}$ from Eq.(1c) and assuming Φ^* to be constant, the roll rate P can be found and used as the roll-rate command P^* as given by the following expression

$$P^* = -(Q\sin\Phi + R\cos\Phi)\tan\Theta - (1/\tau_\Phi)\;(\Phi - \Phi^*) \tag{33}$$

Eq.(A13) can be used to generate P^* both in longitudinal and lateral modes. It can be applied both to the new approach as well as the existing approach [14]. Note that this can be interpreted as a part of the outer loop. For comparison studies incorporating this idea, the time constant $\tau_\Phi = 3$ was set both for the longitudinal as well as for

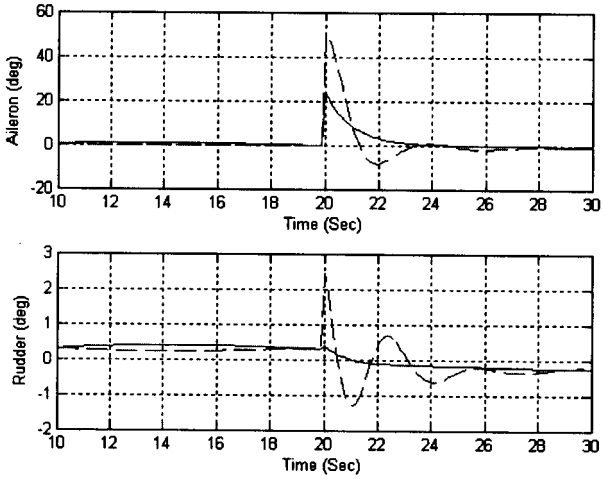

Fig.11 Aileron and Rudder deflections in lateral manuever : zoomed about t=20 sec

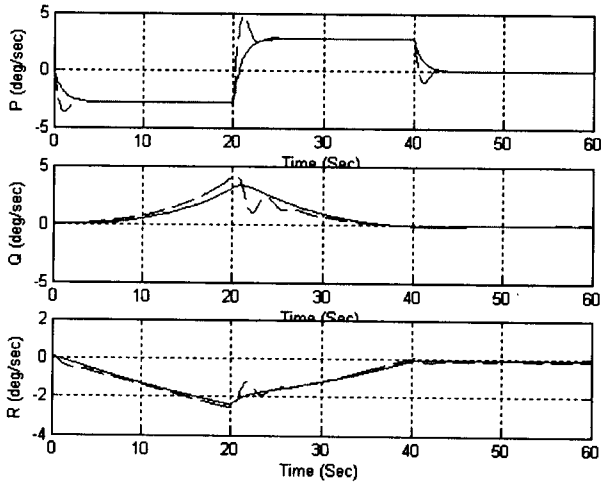

Fig.12 Roll, Pitch and yaw rates in lateral manuever

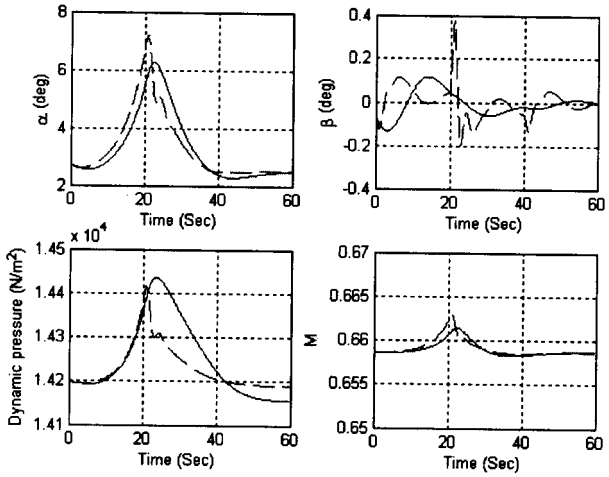

Fig.13 Aerodynamic variables in lateral maneuver

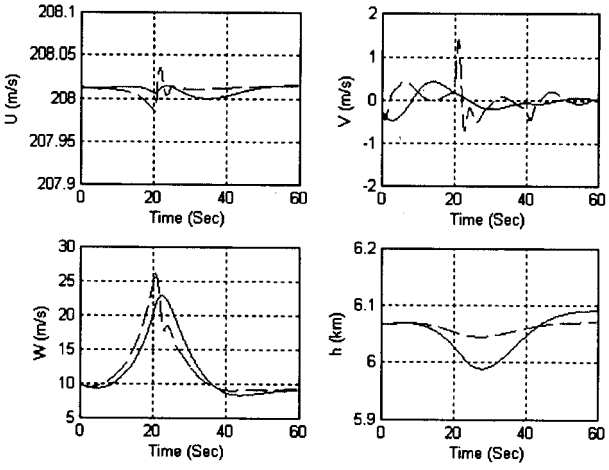

Fig.14 Velocity components and height in lateral maneuver

the lateral case. Trajectories of the tracked states and associated controls for a representative longitudinal maneuver are presented in Figs.16 and 17 respectively and those for a representative lateral maneuver are presented in Figs.18 and 19 respectively. The solid lines correspond to the new approach whereas the dotted lines correspond to the existing approach. In Fig.16 it is clear that the existing approach shows high oscillations in n_z initially which might be too much uncomfortable for the passengers. On the other hand in the new approach the response is smooth and benign (i.e. much less oscillatory). Fig.17 shows that the initial magnitude of the elevator control (main controller in longitudinal maneuvers) in the existing approach is also much higher (double) as compared to the new approach. Besides, the new approach leads to a much smoother elevator control history.

In the lateral case, the response plots for the tracked variables (Fig.18) do not show much of difference. However, in Fig.19 it is evident that the magnitudes of the aileron and rudder controllers (main controllers for lateral case) are much higher initially whenever the bank angle command is changed. To illustrate this clearly, the aileron and rudder control histories of Fig.19 are zoomed about t = 60 Sec in Fig.20. Note that a high aileron value of 40 deg may not be achievable in practice. From a large number of simulation studies it was found that the untracked states remain within reasonable limits.

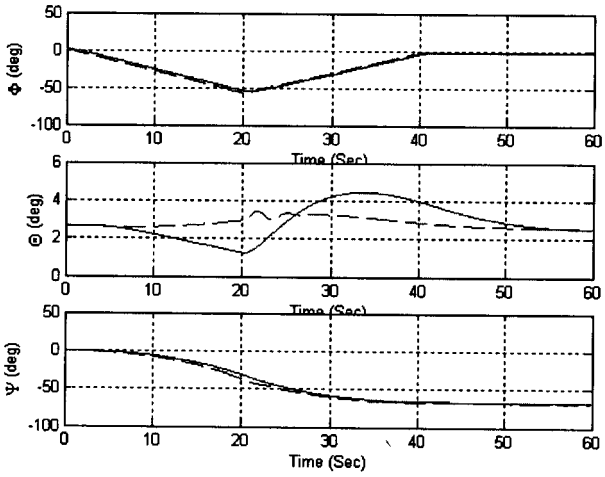

Fig.15 Euler angles in lateral maneuver

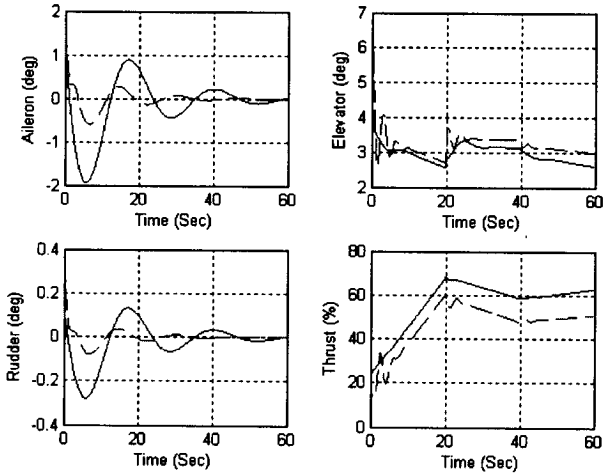

Fig.17 Aileron, Elevator and Rudder deflections and Thrust level in longitudinal maneuver

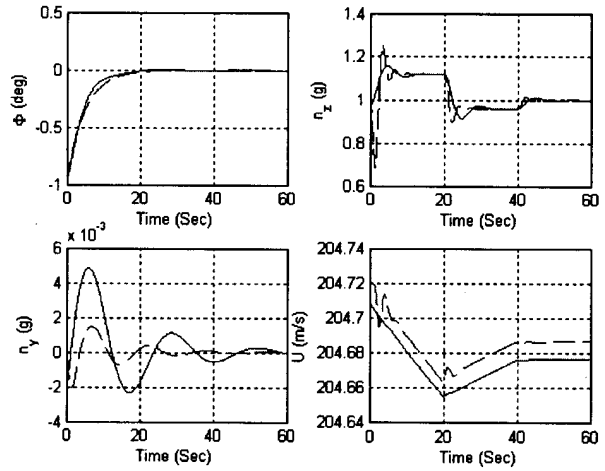

Fig.16 Roll rate, Normal acceleration, Lateral acceleration and forward velocity in longitudinal maneuver

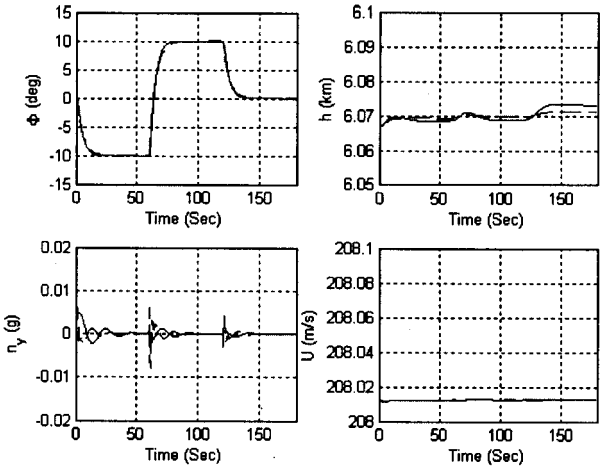

Fig.18 Roll rate, Normal acceleration, Lateral acceleration and forward velocity in lateral maneuver

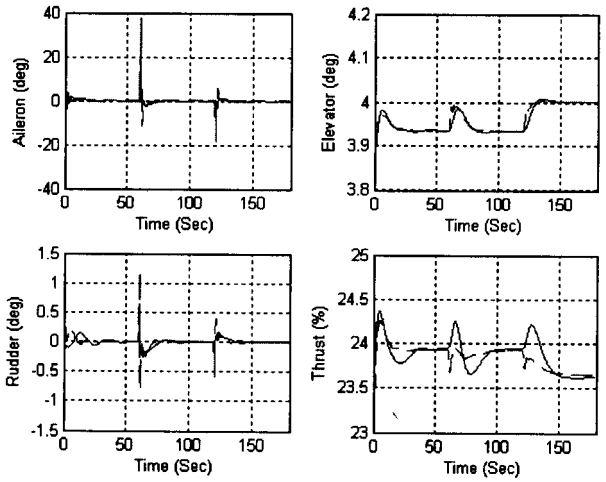

Fig.19 Aileron, Elevator and Rudder deflections and Thrust level in lateral maneuver

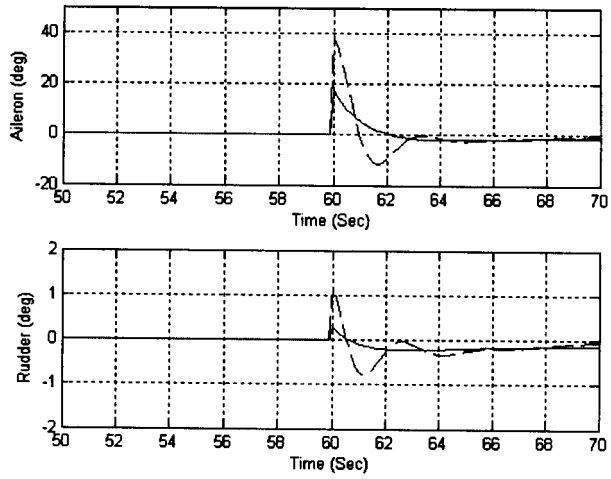

Fig.20 Aileron and Rudder deflections in lateral maneuver : zoomed about t=60 Sec

Conclusions

A new approach based on dynamic inversion technique is presented in this paper for implementation of pilot commands in aircrafts. An important advantage of this approach over an existing approach is that a fewer number of design parameters are needed. The comparison studies support the view that the new approach has a better transient response and demands lower magnitudes of control. These are again desirable features in a controller. Next, an alternative way of computing the roll rate command from the desired bank angle command was also presented. The new approach has a better transient response and demands lower magnitudes of control in this case as well. Note that the Six-DOF simulation studies have been carried out using the limited data available in [16] with respect to Boeing 747 aircraft. This was done mainly because of the difficulty in obtaining a realistic complete envelope of unclassified data for a modern aircraft.

The next logical step would be to test the proposed new method with respect to a fairly complete envelope of data for a modern aircraft (especially for a fighter aircraft as they are inherently unstable). The author intuitively feels that the significant advantages presented in this paper will be preserved in that case as well. However, the research work for such an aircraft is under progress. Promising results for this research, if obtained, will be reported in a separate paper.

References

1. Al-Hiddabi, S.A. and McClamroch, N.H., "Aggressive Longitudinal Aircraft Trajectory Tracking Using Nonlinear Control", Journal of Guidance, Control and Dynamics, Vol.25, No.1, 2002, pp.26-32.

2. Asseo, S. J., "Application of Optimal Control of Perfect Model Following", Journal of Aircraft, Vol.7, July-Aug.,1970, pp.308-313.

3. Bryson, A. E. and Ho, Y. C., "Applied Optimal Control", Taylor and Francis, 1975.

4. Enns, D., Bugajski, D., Hendrick, R. and Stein, G., "Dynamic Inversion: An Evolving Methodology for Flight Control Design", International Journal of Control, Vol.59, No.1,1994, pp.71-91.

5. Ferrari, S. and Stengel, R., "An Adaptive Critic Global Controller", Proceedings of the American Control Conference, 2002, pp. 2665-260.

6. Gupta, S. K., "Numerical Methods for Engineers", Wiley Eastern Limited, 1995.

7. Huang, C. Y. and Stengel, R. F., "Restructurable Control Using Proportional-Integral Implicit Model Following", Journal of Guidance, Control and Dynamics, Vol.13, No.2, 1990, pp. 303-309.

8. Hunt, K. J., "Neural Networks for Control Systems - A Survey", Automatica, Vol. 28, No. 6, 1992, pp. 1083-1112.

9. Jiang, Z. P., "Global Tracking Control of Underactuated Ships By Lyapunov's Direct Method", Automatica, Vol. 38, 2002, pp.301-309.

10. Kaneshige, J., Bull, J. and Totah, J. J., "Generic Neural Flight Control and Autopilot System", Proceedings of the AIAA Conference on Guidance, Navigation and Control, AIAA-2000-4281.

11. Khalil, H. K., "Nonlinear Systems", 3rd Edition, Prentice Hall, 2002.

12. Kim, B. and Calise, A. J., "Nonlinear Flight Control Using Neural Networks", Journal of Guidance, Control and Dynamics, Vol.20, No.1, 1997, pp.26-33.

13. Lane, S. H. and Stengel, R. F., "Flight Control Using Non-Linear Inverse Dynamics", Automatica, Vol.24, No.4, 1988, pp.471-483.

14. Menon, P.K.A., "Nonlinear Command Augmentation System for a High Performance Aircraft", Proceedings of the AIAA Conference on Guidance, Navigation and Control, 1993, AIAA-93-3777-CP.

15. Ngo, A. D., Reigelsperger, W. C. and Banda, S. S., "Multivariable Control Law Design for A Tailless Airplanes", Proceedings of the AIAA Conference on Guidance, Navigation and Control, 1996, AIAA-96-3866.

16. Roskam, J., "Airplane Flight Dynamics and Automatic Controls (Part-I)", Darcorporation, 1995.

17. Slotine, J-J. E. and Li, W., "Applied Nonlinear Control", Prentice Hall, 1991.

18. Soloway, D. and Haley, P., "Aircraft Reconfiguration Using Neural Generalized Predictive Control", Proceedings of The American Control Conference, 2001, pp. 2924-2929.

19. Stevens, B. L. and Lewis, F. L., "Aircraft Control and Simulation": Wiley, 1992.

Appendix

Review of an Existing Method

In this appendix, an existing dynamic inversion approach is described [14]. For convenience we define $X_R \triangleq \begin{bmatrix} P & Q & R \end{bmatrix}^T$, $X_A \triangleq \begin{bmatrix} \Phi & \Theta & \Psi \end{bmatrix}^T$, $X_R^* \triangleq \begin{bmatrix} P^* & Q^* & R^* \end{bmatrix}^T$. With the availability of reference normal and lateral accelerations n_z^*, n_y^* and current state values X, a Command Augmentation System (an outer loop) is first designed. In this step, n_z^*, n_y^* are transformed into equivalent Q^*, R^* as:

$$Q^* = \frac{1}{U}\left[k_1 (n_z^* - n_z) + k_2 \int_0^t (n_z^* - n_z)\, d\tau + (VP - g\cos\Phi\cos\Theta)\right] \quad \text{(A1a)}$$

$$R^* = \frac{1}{U}\left[k_3 (n_y^* - n_y) + k_3 \int_0^t (n_y^* - n_y)\, d\tau + (WP + g\sin\Phi\cos\Theta)\right] \quad \text{(A1b)}$$

where constants $k_1, k_2, k_3, k_4 \in \mathrm{R}^+$ are design parameters (which are supposed to be tuned by the control designer). The values P^*, Q^*, R^* now serve as the commanded reference signals for the Attitude Orientation System (an inner loop). It should be noted that an assumption $\dot{V} = \dot{W} = 0$ is made at this point. X_R^* is then transformed into the rates of the attitude angles as:

$$\dot{X}_A^* = T X_R^* \quad \text{(A2)}$$

where

$$T \triangleq \begin{bmatrix} 1 & \sin\Phi\tan\Theta & \cos\Phi\tan\Theta \\ 0 & \cos\Phi & -\sin\Phi \\ 0 & \sin\Phi\, sec\Theta & \cos\Phi\, sec\Theta \end{bmatrix} \quad \text{(A3)}$$

Using the same kinematics,

$$\dot{X}_A = T X_R \quad \text{(A4)}$$

Differentiating Eq.(A4) with respect to time t and using Eq.(6b), one gets

$$\ddot{X}_A = A_X + B_X U_c \quad \text{(A5)}$$

where

$$A_X \triangleq \dot{T} X_R + T f_R(X), \quad B_X \triangleq T g_R(X) \quad \text{(A6)}$$

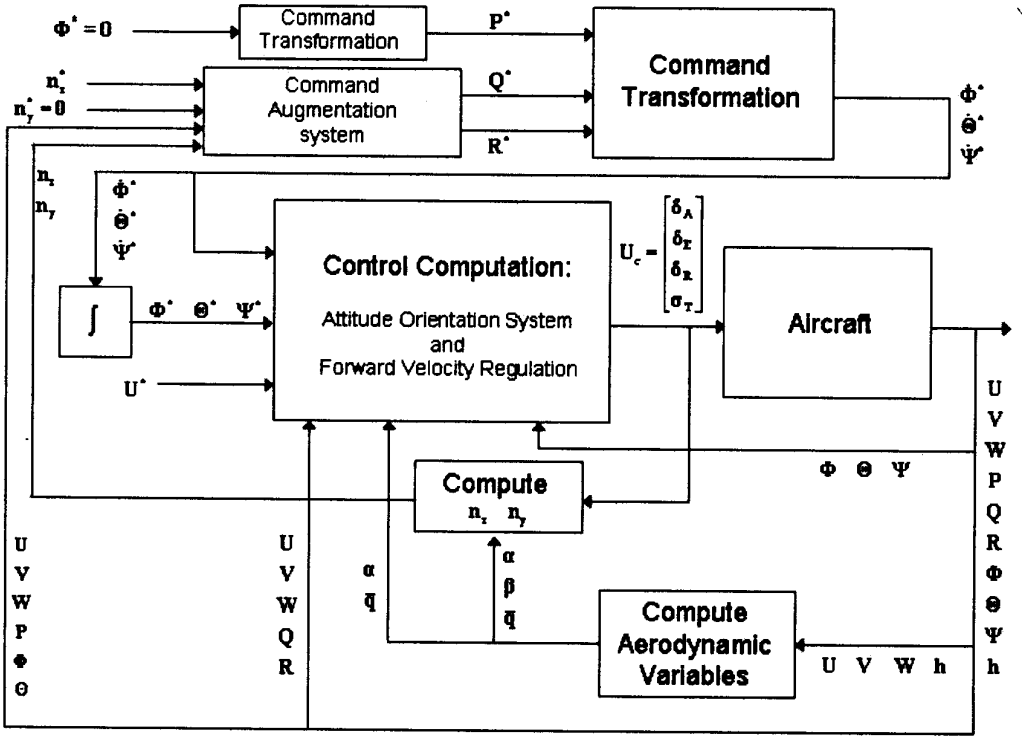

Fig.21 Implementation of the existing technique in longitudinal mode

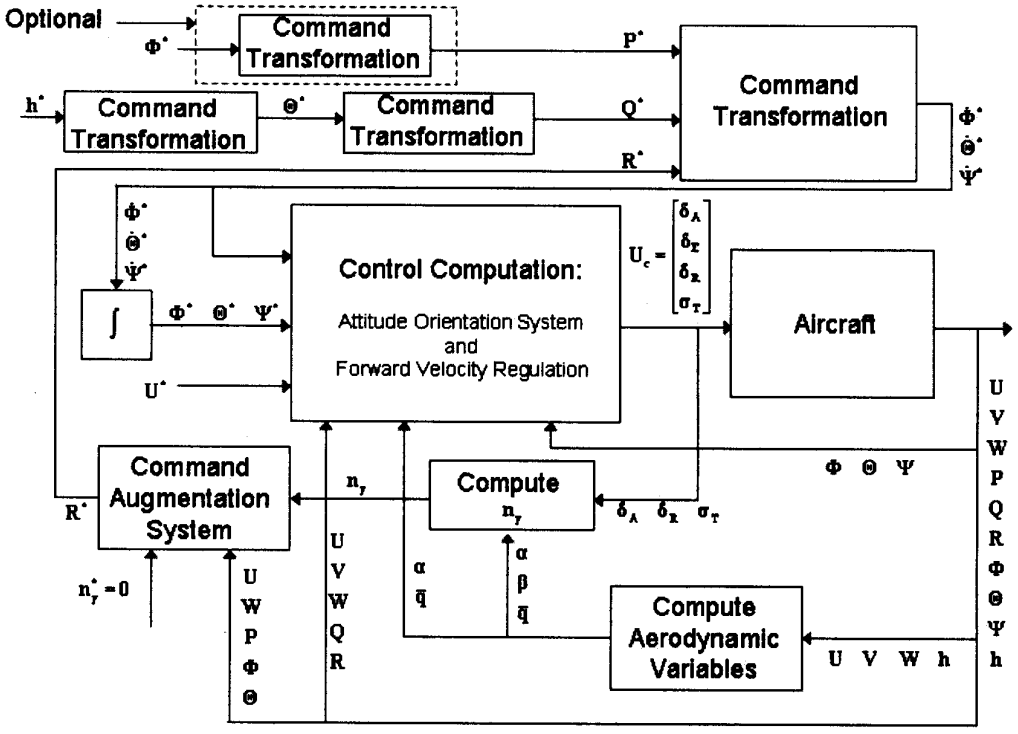

Fig.22 Implementation of the existing technique in lateral mode

Defining the error terms $\hat{X}_A \triangleq \left(X_A - X_A^*\right)$ and $\dot{\hat{X}}_A \triangleq \left(\dot{X}_A - \dot{X}_A^*\right)$ the control is designed such that:

$$\ddot{\hat{X}}_T + K_V \dot{\hat{X}}_A + K_P \hat{X}_A = 0 \tag{A7}$$

where, K_V, K_P are positive definite matrices. One way to choose K_V, K_P is to choose them diagonal with positive entries; i.e. $K_V = diag\ (k_{v_i})$, $k_{v_i} = 2\zeta_i \omega_{n_i}$ and K_P= diag (k_{P_i}), $k_{P_i} = \omega_{n_i}^2$, where $\zeta_i > 0$, $\omega_i > 0$ are the desired damping ratio and natural frequency of the error dynamics of the i^{th} channel respectively. It should be noted that this choice reduces Eq.(A7) to a system of independent scalar equations. Assuming $\ddot{X}_A^* = 0 \left(i.e.\ \ddot{\hat{X}}_T = \ddot{X}_A\right)$ and using Eq.(A5-A7) one gets

$$B_X U_c = -\left\{A_X + K_V \dot{\hat{X}}_A K_P \hat{X}_A\right\} \tag{A8}$$

Since the forward velocity is a tracked variable in this paper, it should be mentioned that the forward velocity tracking is added in the comparison study, which was kept same in this approach as well as in the proposed new approach. After adding the forward velocity related terms, the control expression becomes

$$U_c = -\begin{bmatrix} B_X \\ g_U \end{bmatrix}^{-1} \begin{Bmatrix} A_X + K_V \dot{\hat{X}}_A + K_P \hat{X}_A \\ f_U + (1/\tau_U)\ (U - U^*) - \dot{U}^* \end{Bmatrix} \tag{A9}$$

Implementation of this logic is shown in Figs.21 and Fig.22 for longitudinal and lateral maneuvers respectively. Note that as compared to Figs.1 and 2, these figures are more complicated. Besides we also need to sense the heading angle Ψ of the airplane.